Science of the Total Environment 824 (2022) 153746

Contents lists available at ScienceDirect

Science of the Total Environment

journal homepage: www.elsevier.com/locate/scitotenv

Water vapor adsorption by dry soils: A potential link between the water and carbon cycles

Clément Lopez-Canfin [a,*], Roberto Lázaro [b], Enrique P. Sánchez-Cañete [a,c]

[a] Department of Applied Physics, University of Granada (UGR), Calle Dr Severo Ochoa s/n, Granada, Spain
[b] Department of Desertification and Geo-Ecology, Experimental Station of Arid Zones (EEZA-CSIC), Carretera Sacramento s/n, Almería, Spain
[c] Inter-University Institute for Earth System Research (IISTA-CEAMA), Avenida del Mediterráneo s/n, Granada, Spain

HIGHLIGHTS

- The role of soil water vapor adsorption in drylands carbon cycling remains unclear.
- We explored relationships between water vapor and CO_2 fluxes, and soil properties.
- We used the gradient method to estimate fluxes, and subsequent statistical modelling.
- Our main finding is the existence of a coupling between water vapor and CO_2 fluxes.
- Water vapor adsorption by dry soils could drive the nocturnal CO_2 uptake in summer.

GRAPHICAL ABSTRACT

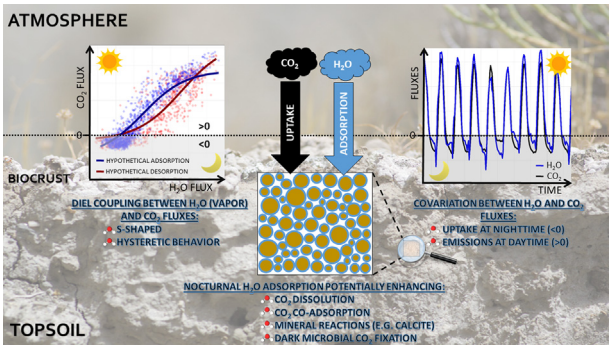

ARTICLE INFO

Article history:
Received 6 October 2021
Received in revised form 2 February 2022
Accepted 4 February 2022
Available online 9 February 2022

Editor: Wei Shi

Keywords:
WVA
Non-rainfall water inputs
CO_2
Carbon dioxide
Biological soil crusts
Biocrusts

ABSTRACT

Water vapor adsorption (WVA) by soil is a potential contributor to the water cycle in drylands. However, continuous in-situ estimates of WVA are still scarce and the understanding of its coupling with carbon cycle and ecosystem processes remains at an incipient stage.

Here we aimed to (1) identify periods of WVA and improve the understanding of the underlying processes involved in its temporal patterns by using the gradient method; (2) characterize a potential coupling between water vapor and CO_2 fluxes, and (3) explore the effect of soil properties and biocrusts ecological succession on fluxes. We assumed that the nocturnal soil CO_2 uptake increasingly reported in those environments could come from WVA enhancing geochemical reactions involving calcite.

We measured continuously during ca. 2 years the relative humidity and CO_2 molar fraction in soil and atmosphere, in association with below- and aboveground variables, over the biocrusts ecological succession. We estimated water vapor and CO_2 fluxes with the gradient method, and cumulative fluxes over the study. Then, we used statistical modelling to explore relationships between variables.

Our main findings are (1) WVA fluxes during hot and dry periods, and new insights on their underlying mechanisms; (2) a diel coupling between water vapor and CO_2 fluxes and between cumulative fluxes, well predicted by our models; and (3) cumulative CO_2 influxes increasing with specific surface area in early succession stages, thus mitigating CO_2 emissions. During summer drought, as WVA was the main water source, it probably maintained ecosystem processes such as microbial activity and mineral reactions in this dryland. We suggest that WVA could drive the nocturnal CO_2 uptake in those moments and discuss biogeochemical mechanisms potentially involved. Additional research is needed to monitor soil water vapor and CO_2 uptake and separate their biotic and abiotic components as those sinks could grow with climate change.

* Corresponding author at: Department of Applied Physics, University of Granada (UGR), Calle Dr Severo Ochoa s/n, Granada, Spain.
E-mail address: lopezcle@ugr.es (C. Lopez-Canfin).

http://dx.doi.org/10.1016/j.scitotenv.2022.153746

1. Introduction

Non-rainfall water inputs (NRWIs) are critical components of the water cycle in drylands (Agam and Berliner, 2006; Wang et al., 2017); in the absence of precipitation, three processes contribute to soil water inputs to the topsoil: (1) fog deposition, (2) dew formation, and (3) water vapor adsorption (WVA). Fog deposition occurs when water vapor pressure reaches saturation, forming water droplets in the air that can deposit on surfaces. Dew formation occurs on a surface when its temperature is lower than or equal to the dew-point temperature of air, at which time the atmospheric water vapor in contact with the surface cools down, reaches saturation and condenses on the surface. WVA occurs when the water vapor pressure of the atmosphere is greater than the water vapor pressure of the soil air, triggering its diffusion from atmosphere towards soil and its retention on the surface of soil particles in a liquid form (water films), through complex physico-chemical mechanisms still not fully constrained (Akin and Likos, 2017). Hence, which NRWI is preponderant in an ecosystem depends on micrometeorological conditions.

In most drylands, atmospheric conditions required for fog formation are rarely met (McHugh et al., 2015). Dew formation was considered until recently as the main NRWI, sometimes exceeding precipitation in amount or frequency, or being the sole source of water for plants and biological soil crusts (Agam and Berliner, 2006). Therefore, dew formation has been extensively studied; however, it has been regularly confounded with WVA and its contribution to the water cycle has probably been overestimated, as favorable thermal conditions for dew deposition are rather uncommon in drylands, particularly on bare soil in hot environments or seasons (Agam and Berliner, 2006). In comparison, WVA by soil has received little attention despite the fact that it can occur on a more regular basis, even when soil surface temperature is greater than dew point temperature. It is now considered as a likely substantial contributor to the water cycle in drylands (McHugh et al., 2015), which cover about 41% of the Earth's terrestrial surface. Moreover, since warmer air has the capacity to hold more water vapor, and soil drying is predicted with high confidence in some regions of the globe (Collins et al., 2013), WVA by soil might be enhanced by climate change.

In spite of the potential global importance of WVA, in situ estimates of the process are still very scarce. Only few studies aimed to monitor WVA fluxes and they were almost always restricted to short time periods (Agam and Berliner, 2006; Kosmas et al., 2001; Uclés et al., 2015; Verhoef et al., 2006), with few exceptions (Kohfahl et al., 2021; Saaltink et al., 2020). That is partly due to a methodological gap as traditional approaches to estimate WVA fluxes include either complex numerical modelling using numerous parameters that require substantial effort to collect, or expensive lysimeters that can disturb the natural soil profile and pedoclimatic conditions. By contrast, the gradient method that has been increasingly used recently to determine soil-atmosphere greenhouse gases fluxes (Maier and Schack-Kirchner, 2014; Sánchez-Cañete et al., 2017) could represent a suitable approach to obtain estimates of WVA as it is easy to deploy, generates only limited soil perturbation, and can provide long-term continuous measurements and further understanding of the belowground mechanisms involved in WVA.

The gradient method is based on the main assumption that molecular diffusion is the dominant gas transport process between soil and atmosphere, a condition that is generally considered to be fulfilled both for CO_2 (Šimůnek and Suarez, 1993) and water vapor (Liu et al., 2020). The only drawback of this method is that the estimated flux is highly dependent on the chosen coefficient of diffusion and therefore, it is recommended to apply a site-specific calibration to improve the accuracy of the flux estimation. For CO_2, this calibration can be performed with soil chamber measurements (Sánchez-Cañete et al., 2017). However, for water vapor, no standardized procedure exist yet as soil-atmosphere diffusive fluxes of water vapor have seldom been estimated and most studies were limited to laboratory experiments (e.g. Jabro, 2008; Rao and Rekapalli, 2020; Reyzabal and Bazán, 1992). Only one study estimating those fluxes in-situ was found in the literature (Bittelli et al., 2008). If a substantial contribution of WVA to the water cycle in drylands were confirmed by more observational studies including accurate continuous monitoring, the process could potentially impact other element cycles and ecosystem processes, as they are strongly constrained by water availability in those environments.

In particular, the understanding of the coupling between WVA, carbon cycle and ecosystem processes remains at an incipient stage; nevertheless, WVA could enhance water-limited microbial activity and mineral reactions in drylands. For example, some lichens have the capacity to use water vapor (Lange et al., 1994, 1992; Zheng et al., 2018). A previous study found that WVA increased soil CO_2 production revealing that dryland microorganisms were able to use this water input to sustain their metabolic activity (McHugh et al., 2015). Other studies reported that dew contributed to rock weathering and karst development in drylands (Agam and Berliner, 2006). Therefore, WVA is also expected to be a weathering agent of soil minerals. In particular, WVA on calcite is energetically favorable (Rahaman et al., 2008) and can lead to the formation of carbonate species and reorganization of the mineral surface (Rubasinghege and Grassian, 2013). Since microbial and mineral (e.g. calcite) processes can produce/consume CO_2 via respiration/assimilation and precipitation/dissolution respectively, the enhancement of those processes by WVA is likely to affect the soil-atmosphere CO_2 exchange in drylands.

Nocturnal CO_2 uptake by soil has been increasingly reported in water-limited ecosystems (Fa et al., 2016; Hamerlynck et al., 2013; Ma et al., 2013), including at our study site (Lopez Canfin et al., n.d.), and its origin remains debated (Sagi et al., 2021); different abiotic forces have been suggested to drive the phenomenon but the potential effect of WVA on both biotic and abiotic components of the ecosystem has not been explored yet. On the one hand, drylands shelter a rich biodiversity of biological soil crusts (hereafter, biocrusts), key ecosystem engineers that sustain many important ecological functions including an ability to fix CO_2 by photosynthesis. In addition, there is growing evidence that among those communities, chemotrophs able to perform CO_2 fixation in the dark coexist with phototrophs (Bay et al., 2021; Liu et al., 2021). On the other hand, the abiotic assumption of calcite dissolution consuming CO_2 to explain the nocturnal CO_2 uptake by soil has been challenged by the supposition that, since the geochemical reaction consumes water, such uptake should not occur in dry soils (Schlesinger et al., 2009). This is without considering WVA as a potential link between the water and carbon cycle in drylands. Biotic and abiotic processes could also be tightly coupled, as microorganisms such as *Cyanobacteria* or fungi can for example promote the dissolution of $CaCO_3$ (Garcia-Pichel et al., 2010; Tian et al., 2021).

Assessing the role of WVA in drylands requires improved characterization of its drivers in-situ. The amount of adsorbed water in the soil depends on the magnitude of the soil-atmosphere vapor gradient, and the total surface area of soil particles (Kool et al., 2021). Since clay particles have the largest surface area, the amount of adsorbed water generally increases with the soil clay content; the clay type also affects the amount of adsorbed water as surface area varies between clay types (Agam and Berliner, 2006). Soil organic carbon content and salinity have been reported as well as factors controlling WVA (Amer, 2019; Arthur et al., 2020). However, to our knowledge, the soil content in gypsum, a common salt at Earth surface, has never been investigated as a potential driver of soil-atmosphere water vapor fluxes; gypsum is more soluble than calcite and has strong hydration/dehydration properties, with dehydration starting at ca. 40 °C (Azimi et al., 2007), a temperature range that can be easily reached in drylands topsoil.

In this research we aimed to (i) identify periods of WVA and improve the understanding of the underlying processes involved in its temporal patterns by using the gradient method; (ii) characterize a potential coupling between water vapor and CO_2 fluxes; and (iii) explore the effect of soil properties and biocrusts ecological succession on fluxes. We assumed that (i) the gradient method could be used to measure the diffusion of water vapor from atmosphere to soil, considering those influxes as proxies of WVA; WVA should be substantial during the dry period due to enhanced soil drying during daytime, magnifying the soil-atmosphere water vapor pressure gradient; (ii) fluxes of water vapor and CO_2 could be tightly

coupled. In particular, WVA was expected to be the underlying process controlling nocturnal CO_2 uptake; and (iii) soil surface area, gypsum content and biocrusts ecological succession could significantly affect WVA.

2. Material and methods

2.1. Experimental site

This study was conducted in the experimental site of El Cautivo, an area of badlands located in the Tabernas Desert (Almería, Spain) (Fig. S1). The climate is classified as semi-arid thermo-Mediterranean with a mean annual temperature of 17.9 °C and an average annual precipitation of ca. 230 mm with great inter-annual variation (coefficient of variation (CV) of 36%) and intra-annual variation (CV of up to 207%) based on a 30-year rainfall record from 1967 to 1997 (Lázaro et al., 2004, 2001). The piezometric level in the area oscillates between 22 and 26 m depth (data from 1985 to 2020 of the Spanish Geological Survey, IGME). The bedrock horizon starts at a depth ranging from ca. 0.5 to 1.5 m and consists of gypsum-calcareous mudstones and calcaric sandstones deposited during the Miocene. Soils in the area are mainly Epileptic and Endoleptic Leptosols, Calcaric Regosols and Eutric Gypsisols (FAO, 1998), and the soil texture is silty-loam, dominated by gypsum-calcareous and siliceous particles of silt-size (>60%); fine sand ranges from 20% to 35%, and clay ranges from 5% to 10%; a detailed pedological characterization of the soil horizons can be found in Cantón et al. (2003). Bare soil, eroded or originated from sediment deposition, occupies a third of the territory, another third is covered by short vascular vegetation with biocrusts in the interspaces and the rest is covered mainly by biocrusts' (Lázaro et al., 2000). Different biocrust types can be distinguished and associated with stages of ecological succession (Lázaro et al., 2008): (1) physical depositional crust (PD); (2) incipient *Cyanobacteria* (IC); (3) mature *Cyanobacteria* (MC); (4) lichen community dominated by *Squamarina lentigera* (Web.) Poelt and *Diploschistes diacapsis* (Ach.) Lumbsch (SD); and (5) lichen community characterized by *Lepraria isidiata* (Llimona) Llimona & Crespo (LI).

2.2. Environmental measurements and soil analyses

Continuous measurements of soil and above-surface variables were conducted from February 2018 to December 2019 (see experimental design in Fig. 1). At 5 cm depth, the CO_2 molar fraction (χ_c) of soil was measured mainly by GMP252 probes (accuracy of ±2% of reading in the range 0–10,000 ppm) and some measurements were completed with GMM222 transmitter modules (accuracy of ± (1.5% of the range + 2% of reading in the range 0–10,000 ppm)) (Vaisala, Vantaa, Finland). The soil water content (ϑ_w) was measured by EC-5 and 5TM sensors (Meter Group, Pullman, WA, USA). The ϑ_w sensors were calibrated according to the general equation for mineral soils provided by the manufacturer. This equation should apply for all mineral soils up to an electrical conductivity (EC) of 8 dS m^{-1} in saturation extract according to the instructions of the manufacturer. Preliminary tests showed that most soils at our study site had an EC < 1 dS m^{-1} in 1:5 soil to water ratios. Based on those values, it was reasonable to expect that EC in saturation extracts would not exceed the recommended threshold (Kargas et al., 2020).

The 5TM sensors also measured the soil temperature (T_s); T_s measurements were also replicated with thermistors (108, Campbell Scientific, Logan, UT, USA; hereafter CSI). All such measurements were performed within each stage of biocrusts succession, in triplicates. They were also performed in mature cyanobacterial patches within the SD microsite (MC2; in duplicate). The maximum distance between microsites was ca. 500 m. Within each site, the relative humidity in soil at 5 cm depth and in atmosphere in contact with soil (RH_s and RH_a, respectively) were measured by iButton® DS1923 logger (accuracy of ±5% of reading in the range 0–100%) (Maxim Integrated, San Jose, CA, USA); air temperature (T_a) and atmosphere relative humidity at 30 cm aboveground were measured by a S-THB-M00x Smart Sensor (Onset Computer Corporation, Bourne, MA, USA; hereafter Onset); the surface temperature (T_{surf}) was measured by a S-TMB-M0xx Smart Sensor (Onset) and the photosynthetically active radiation (PAR) by a S-LIA-M003 Smart Sensor (Onset); precipitation was measured by a Rain-O-Matic-Pro tipping-bucket rain gauge of 0.25 mm resolution (Pronamic, Ringkoebing, Denmark) at 1.5 m above the ground surface. At 2 cm aboveground, the χ_c, of atmosphere (same sensors as soil χ_c) was monitored in the PD and SD microsites, and atmospheric pressure was monitored in the LI microsite. The rain gauge was connected to an on–off Hobo Event data logger (Onset) and all other variables were measured every 30 s and stored as 20-minute averages by data-loggers CR1000 (CSI) and H21 (Onset). A summary of the continuous environmental measurements and associated instruments is provided in Table S1.

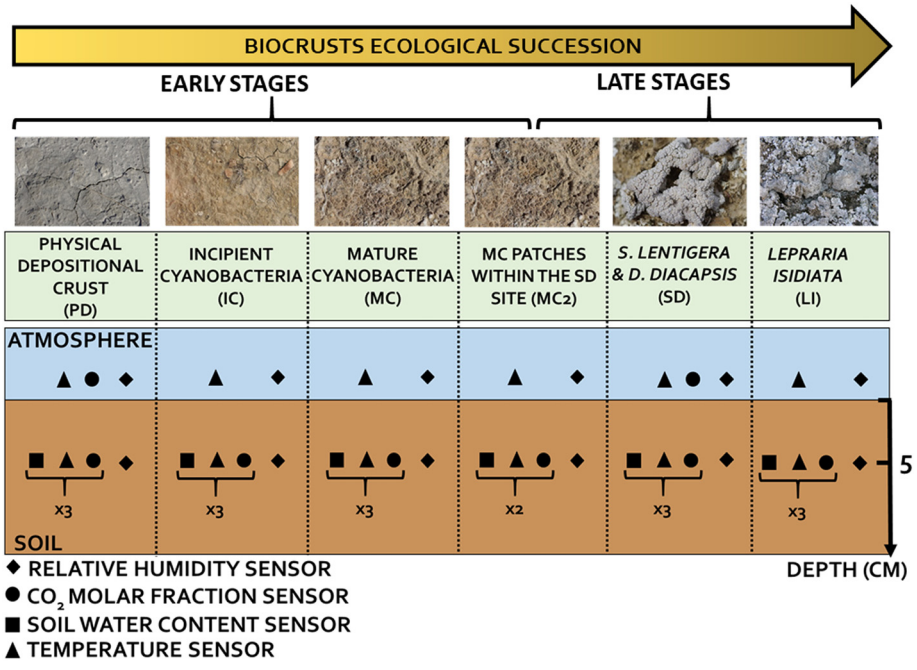

Fig. 1. Experimental design.

The soil CO_2 efflux (F_c) was measured regularly (for 14 days in total) with a non-steady-state through-flow chamber (EGM-4, PP-system, Amesbury, MA, USA), also known as closed dynamic chamber. To this end, a PVC collar of 0.0069 m^2 surface area was inserted into the soil close to each soil χ_c probe. We took the precaution of inserting gently the collar in order to limit soil and crust disturbance and measurements were started one month later to allow for the recovery of soil surface. During measurements, the portable chamber was placed over the soil collar and the flux was calculated from the rate of linear change in the chamber CO_2 molar fraction measured every 3 s over 120 s; measurements were irregularly spaced in time, trying to cover the natural range of ϑ_w variability.

In the topsoil (0–5 cm), the porosity (ϕ), the soil total specific surface area (SSA_s), gypsum content, calcium carbonate equivalent content (CCE), calcite reactive surface area (RSA), calcite specific surface area (SSA_c, calcite RSA per weight of calcite) and soil organic content (SOC) were measured within each microsite described above. The SSA_s was estimated from the particle size distribution measured by a laser particle size analyzer (Mastersizer 3000 Hydro EV, Malvern Panalytical, Malvern, United Kingdom), assuming that the particles were spherical and non-porous. The SOC content was measured by a modified wet oxidation method (Mingorance et al., 2007) and determined with a spectrophotometer (Spectronic Helios Alpha 9423 UVA 1002E, Thermo Fisher Scientific, Waltham, MA, USA). The gypsum content was determined by exploiting the gypsum-bassanite phase change (Lebron et al., 2009). The CCE and RSA were quantified by measuring the CO_2 released during an acidic reaction (Lopez-Canfin et al., 2021).

2.3. Data processing, water vapor and CO_2 fluxes calculation

Hourly averages were calculated on the data. To fill data gaps and enable the modelling of time series as well as the determination of cumulative fluxes, the dataset was split into subsets of variables of the same type (e.g. temperatures) and each subset was imputed separately to avoid generating spurious correlations. A non-parametric method based on random forests was used to replace missing values in each subset (Stekhoven and Bühlmann, 2012).

The water vapor pressure in soil and atmosphere was calculated as:

$$P_h = \frac{RH}{100} P_s \tag{1}$$

where P_h is the water vapor pressure (kPa), RH is the relative humidity (%) measured with the iButton® DS1923 loggers and P_s is the saturation water vapor pressure calculated according to Buck (1981) using the air temperature measured with the S-THB-M00x Smart Sensor (since it was protected against direct radiation and radiative cooling) and the soil temperature measured with the iButton® DS1923 logger.

The water vapor molar fraction in soil and atmosphere was calculated as:

$$\chi_h = \frac{P_h}{P_a} \tag{2}$$

where χ_h is the water vapor molar fraction (mol mol^{-1}, or kPa based on to Dalton's law) and P_a is the atmospheric pressure (kPa).

The measured χ_c in soil and atmosphere were corrected internally by the CO_2 sensor for real-time changes in temperature (in soil and atmosphere, respectively) as well as in post-processing for real-time changes in atmospheric pressure as:

$$\chi_{c\ (corrected)} = \chi_{c\ (measured)} \frac{P_0}{P_a} \tag{3}$$

where P_0 is the reference pressure (101.325 kPa).

The soil-atmosphere fluxes of water vapor (F_h) and CO_2 (F_c) were calculated according to the gradient method based on the first Fick's law of molecular diffusion:

$$F = -\rho_a k_s \frac{d\chi}{dz} \tag{4}$$

where F is the soil-atmosphere flux (mmol m^{-2} s^{-1} and μmol m^{-2} s^{-1} for F_h and F_c, respectively), ρ_a is the average molar density of air (mol m^{-3}), $d\chi$ is the gradient in water vapor or CO_2 molar fraction (mmol mol^{-1} and μmol mol^{-1}) between atmosphere and soil, and dz is the vertical gradient between atmosphere and soil (m), k_s is the diffusion coefficient or empirical soil transfer coefficient (m^2 s^{-1}).

As k_s is a major source of uncertainty in the diffusive flux calculation, it is recommended to apply a site-specific calibration to improve the accuracy of the gradient method (Sánchez-Cañete et al., 2017). Therefore, the k_s of F_c was calibrated from 225 chamber measurements by rearranging Eq. (4):

$$k_s = -\frac{F_{soil}\, dz}{\rho_a\, d\chi} \tag{5}$$

where F_{soil} are the CO_2 fluxes measured with the soil chamber measurements.

Since k_s is generally considered to depend on the diffusion coefficient of CO_2 in free air and the air-filled pore space (ϑ_a, equal to *soil porosity* – ϑ_w), then k_s was modelled as a function of these variables. The following model provided the best fit to the data and therefore was retained for the CO_2 flux estimation:

$$k_s = D_a a e^{b\theta_a} \tag{6}$$

where a and b are empirical coefficients obtained by non-linear least squares regression (0.07 and 3.17, respectively), and D_a is the diffusion coefficient of CO_2 in free air calculated according to Jones (1992):

$$D_a = D_{a,0} \left(\frac{T}{T_0}\right)^{1.75} \left(\frac{P_0}{P_a}\right) \tag{7}$$

where $D_{a,0}$ is the diffusivity of CO_2 in air (1.47 10^{-5} m^{-2} s^{-1}), T is the measured soil temperature, T_0 is 293.15 K and P_0 is 101.325 kPa.

For the estimation of F_h, since no standardized procedures exist yet to calibrate k_s, the coefficient was calculated according to the only in-situ study found in the literature (Bittelli et al., 2008):

$$k_s = D_a \beta \theta_a^m \tag{8}$$

where D_a is the diffusion coefficient of water vapor in free air calculated according to Jones (1992) using $D_{a,0}$ of water vapor (2.4 10^{-5} m^{-2} s^{-1} according to Campbell and Norman (1998)), and β and m are constants that account for the shape of soil particles. Values of 0.9 and 2.3 were used for the later parameters, respectively, as according to Bittelli et al. (2015), those values are good approximations for undisturbed samples.

For comparative purpose of the resulting F_h, k_s was also calculated according to Xu et al. (1992) as:

$$k_s = D_a \frac{\theta_a^{2.58}}{\varphi^2} \tag{9}$$

where φ is the soil porosity.

The uncertainty in the estimation of F_h fluxes was calculated from the accuracy of the RH sensors used to calculate those fluxes. The following cumulative F_h and F_c were calculated from the data: effluxes, influxes and total fluxes. They refer to, respectively: positive fluxes (emissions, from soil to atmosphere), negative fluxes (uptake, from atmosphere to soil) and the sum of both fluxes (positive and negative).

2.4. Statistical modelling

All analyses were performed with R software v.3.6.3 and the significance level was set to 5%. The statistical protocol of Zuur and Ieno (2016) was used to analyze the data. Our model construction aimed to answer the following two questions: 1) is there a coupling between F_h and F_c, and in particular, is F_h a good predictor of F_c? and 2) Do soil variables (especially specific surface area and gypsum content) and biocrusts ecological succession significantly affect those fluxes?

We fitted models from both diel and cumulative fluxes over the study. For the former, the dataset was first split into a training set (first year) for calibration and a testing set (second year) for cross-validation. We selected only data from the summer season to exclude the effect of precipitation. Preliminary data exploration revealed a hysteretic relationship between F_h and F_c on a diel scale, presumably modellable with two sigmoid functions: one for the diel decrease in F_c and F_h from their maximum during daytime to their minimum at night, and vice-versa for the diel increase in those variables (Fig. S2B). Therefore, we additionally split the data into diel "decrease" and "increase" subsets, based on the average hour of minimum and maximum F_h, in order to model each part of the hysteresis independently. Since the "S-shapes" exhibited substantial variation between crust types and replicates, non-linear mixed models were fitted (Pinheiro and Bates, 2000). This approach allowed the parameters of the model to vary both with the fixed effect "crust type" and the random effect "replicate". The following four-parameter logistic model was chosen to model F_c as a function of F_h:

$$F_c = \varphi_1 + \frac{\varphi_2 - \varphi_1}{1 + \exp\left[(\varphi_3 - F_h)/\varphi_4\right]} \quad (10)$$

where ϕ_1 is the horizontal asymptote as $F_h \to \infty$, ϕ_2 the horizontal asymptote as $F_h \to -\infty$, ϕ_3 the F_h value at the inflection point of the sigmoid (the value of F_h for which the response variable $F_c = \phi_1/2$), and ϕ_4 a scale parameter on the *x*-axis. Further information about this type of model, including a graphical visualization of the parameters, is available in Pinheiro and Bates (2000). The serial correlation inherent to time series was modelled with a first-order autoregressive (AR1) process within each day.

Using a simple visual inspection of the time series, it was not clear whether the variation in F_h tended to lead or lag the variation in F_c. In general, negative F_h and F_c fluxes seemed to occur almost simultaneously but depending on the period and location, the variation in F_h could sometimes apparently lead or lag the variation in F_c. Therefore, a cross-correlation analysis was performed to determine whether F_c or F_h tended to lead or lag. In addition, relationships between pairs of variables were explored, and modelled either by linear or non-linear regression. All linear models' assumptions on residuals were checked with statistical tests: the Durbin-Watsons, Breusch-Pagans, and Shapiro-Wilks tests were used to assess independence, homoscedasticity, and normality, respectively. Non-linear models assumptions on residuals were checked visually.

3. Results

3.1. Temporal dynamics

3.1.1. General trends

In all stages of the biocrusts ecological succession, the soil relative humidity (RH_s) decreased sharply during summer drought (see for example in the mature *Cyanobacteria* microsite, Fig. 2A). During this period characterized by the absence of precipitation, soil water content minima (Fig. 2E) and temperature maxima (Fig. 2F), RH_s became regularly lower than atmosphere relative humidity (RH_a). However, during this summer period, soil temperature (T_s) and atmosphere temperature (T_a) diverged substantially, with T_s exceeding T_a (Fig. 2F). Warmer air increases the saturation water vapor pressure, i.e. the capacity of air to store water vapor. Therefore, the molar fractions of water vapor (χ_h) were more relevant to understand the underlying processes involved in temporal patterns of water vapor fluxes (F_h), also because they were directly used to calculate F_h based on the gradient method. During summer drought, atmosphere χ_h regularly exceeded soil χ_h (Fig. 2B). Such conditions were often favorable to the inversion of the water vapor pressure gradient, thus generating negative F_h (Fig. 2C). Note that during another dry period but this time marked by winter temperatures (Fig. 2E and F), negative F_h fluxes were almost inexistent (Fig. 2C). Negative F_h always occurred at values of $RH_a > 40\%$ (see for example in the mature *Cyanobacteria* microsite, Fig. S3) but not exclusively, as positive F_h were also found in that interval. The conditions necessary for dew formation (i.e. T_{surf} < dew point) and fog formation (i.e. $RH_a = 100\%$) were uncommon in summer (see example in Fig. 3E, and Fig. 2A, respectively).

During a complete hydrological year from 01/09/2018 to 31/08/2019, the amount of water accumulated by precipitation was 174 mm while the amount of water accumulated through negative F_h ranged from 0.37 ± 0.02 mm to 1.58 ± 0.08 mm (i.e. from 0.21 ± 0.01% to 0.91 ± 0.05% of precipitation, respectively), depending on the microsite, using the model of Bittelli et al. (2015) to calculate the diffusion coefficient of water vapor between soil and atmosphere. By contrast, using the diffusion model of Xu et al. (1992), negative F_h accounted for between 1.42 ± 0.07 and 4.91 ± 0.25 mm, i.e. 0.82 ± 0.04% to 2.82 ± 0.14% of the annual precipitation over the same period. The amount of water accumulated through negative F_h only during summer of the same hydrological year ranged from 0.17 ± 0.01 mm to 1 ± 0.05 mm with the first model and from 0.67 ± 0.03 mm to 3.62 ± 0.18 mm with the second model. The amount of water accumulated through negative F_h only during summer represented between 47 and 75% of the annual negative F_h regardless of the diffusion model. By contrast with negative F_h that occurred predominantly during summer, negative CO_2 fluxes (F_c) occurred throughout the study period, with a slightly lower magnitude in summer (see for example in the mature *Cyanobacteria* microsite, Fig. 2D). The cumulative evaporation (positive F_h) ranged from 7.40 ± 0.37 mm to 15.21 ± 0.76 mm (i.e. from 4.25 ± 0.21% to 8.74 ± 0.44% of precipitation) based on the diffusion model of Bittelli et al. (2015). It ranged from 23.02 ± 1.15 mm to 53.72 ± 2.69 mm (i.e. from 13.23 ± 0.66% to 30.87 ± 1.55% of precipitation) based on the diffusion model of Xu et al. (1992).

The ratio of cumulative negative F_h to cumulative positive F_h over the whole study period tended to increase over biocrusts succession (3%, 3%, 9%, 7%, 11% and 15% for the PD, IC, MC, MC2, SD and LI microsites, respectively). The average soil-atmosphere gradient of water vapor molar fraction decreased over succession (14.5, 12.5, 11.7, 10.6, 9.4, and 7.3 mmol mol^{-1} for the PD, IC, MC, MC2, SD and LI microsites, respectively).

3.1.2. Diel patterns in water vapor and CO_2 fluxes

A more detailed representation of the previously mentioned periods of summer and winter drought, during which negative F_h were respectively common and virtually absent, is provided in Fig. 3. During summer, negative F_h occurred due to a decrease in soil χ_h during the afternoon (reaching minima at nighttime) and a concomitant increase in atmosphere χ_h at nighttime inverting the soil-atmosphere water vapor pressure gradient (Fig. 3C). During winter, soil χ_h was lower in average but followed the same diel pattern whereas atmosphere χ_h was also lower in average but usually did not increase enough at nighttime to invert substantially the gradient (Fig. 3D). It is also worth noting that RH_s presented the opposite diel pattern to soil χ_h (Fig. 3A and B) and that the soil χ_h decrease during the afternoon and overnight (Fig. 3C and D), occurred in synchrony with a decrease in temperature (Fig. 3E and F) and PAR (Fig. 3G and H). In addition, brief positive excursions in χ_h were frequently observed at sunrise, particularly in summer (Fig. 3C).

During summer, F_c and F_h covaried and used to be both negative at night (Fig. 4). The cross-correlation analysis revealed that overall, the variation in F_h slightly led the variation in F_c, i.e. by 1 h (1 h being the maximum time resolution of the data). The moment when fluxes became negative used to coincide exactly with PAR reaching the zero value (Figs. 3G and 4), due to the inversion of the gradient of water vapor molar fractions at this moment (Fig. 3C).

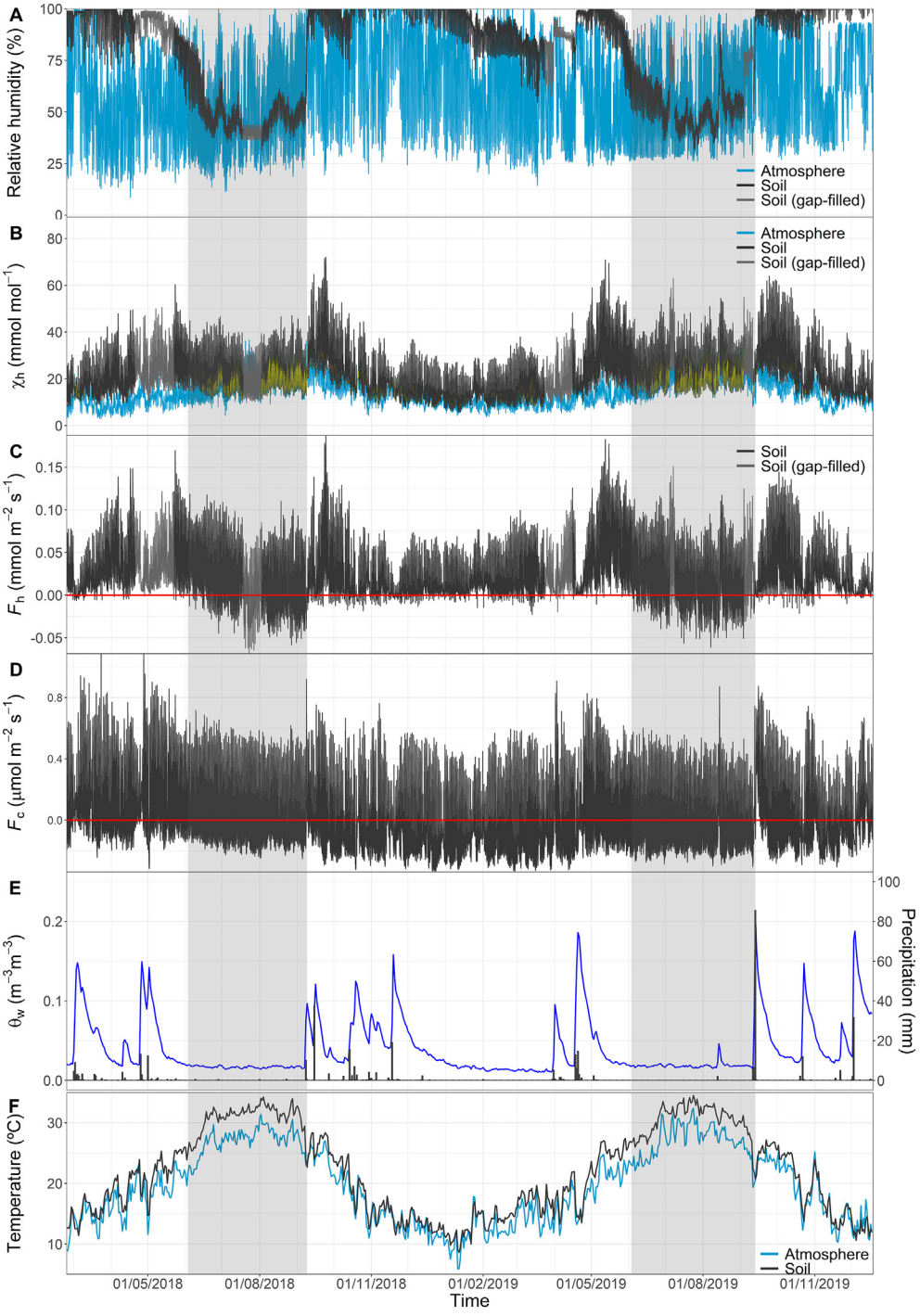

Fig. 2. Time series of (A) hourly relative humidity in soil and atmosphere (B) hourly water vapor molar fraction (χ_h) in soil and atmosphere. The yellow areas delimit moments during which atmosphere χ_h exceeds soil χ_h; (C) hourly soil-atmosphere water vapor flux (F_h); (D) hourly soil-atmosphere CO_2 flux (F_c); (E) daily soil water content (ϑ_w, blue line) and precipitation (black bars); (F) daily temperature of soil and atmosphere. All-time series come from the mature *Cyanobacteria* microsite. The shaded area highlights periods of consistent negative F_h during summer drought.

There was a diel hysteresis between F_c and T_s as well as between F_c and F_h (Fig. S2A and B, Fig. 5A). The former was difficult to model whereas the latter could be modelled with two sigmoidal functions, one for the diel decrease from F_h maximum to F_h minimum and vice-versa for the diel increase (Fig. 5A, supporting information Table S2A). Note that in all succession stages, the diel "decrease" path of the observed hysteresis was on average longer than the diel "increase" path. The ratio of diel decrease time over diel increase time ranges from 1.6 in the PD and IC microsites to 3 in the LI site. After calibration of the model on the first summer of data, the model was cross-validated with predictions on the second summer of data, which showed overall good performance (Fig. 5B and C).

3.2. Relations between cumulative water vapor and CO_2 fluxes, soil properties and biocrusts succession

There was a significant negative linear relationship ($p < 0.001$, adjusted $R^2 = 0.68$) between cumulative F_c and F_h estimated on the whole study period (Fig. 6). Mature *Cyanobacteria* microsites exhibited the least CO_2

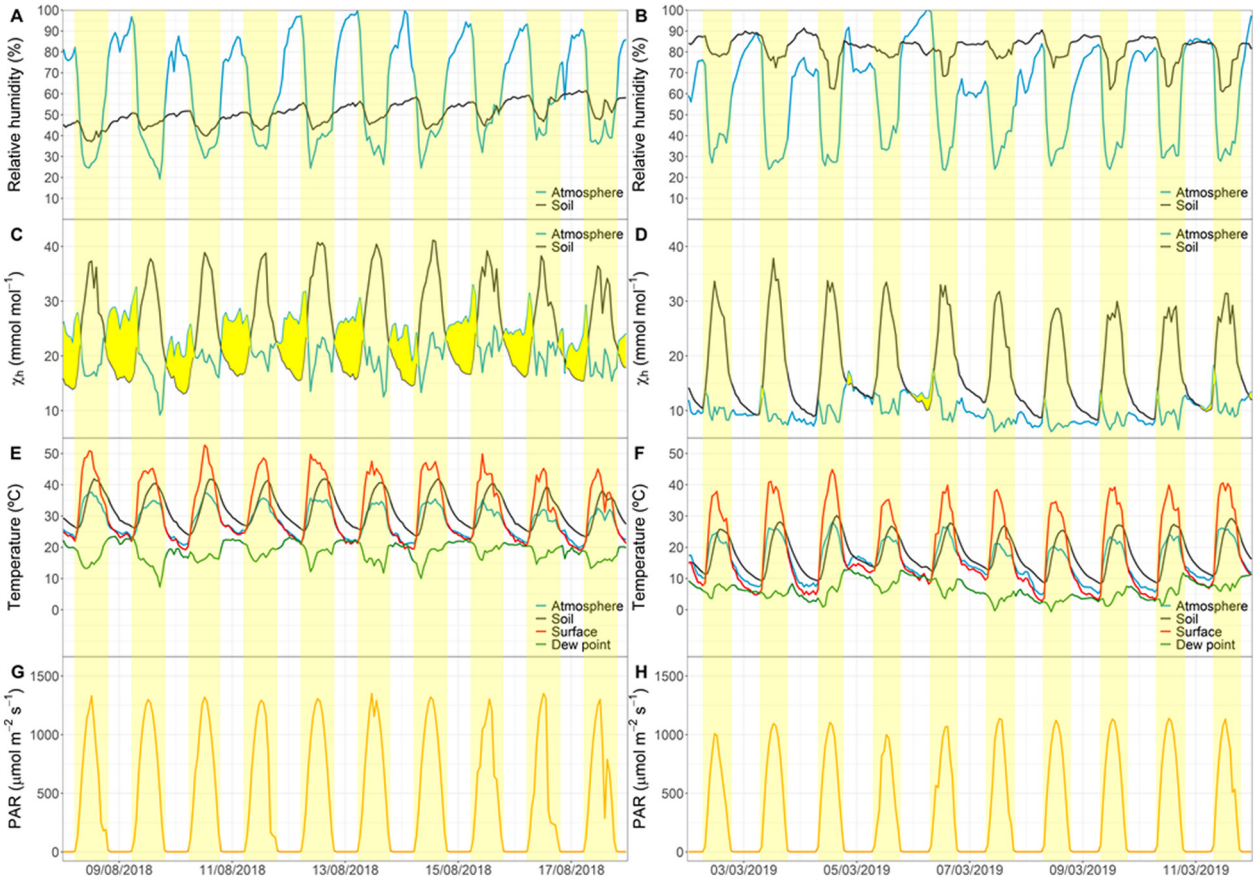

Fig. 3. Variation of environmental variables over time during a drought period in summer (left column) and winter (right column); (A and B) relative humidity in soil and atmosphere; (C and D) molar fraction of water vapor (χ_h) in soil and atmosphere. The yellow area delimits moments during which atmosphere χ_h exceeds soil χ_h, leading to negative soil-atmosphere water fluxes, i.e. from atmosphere to soil; (E and F) temperature of soil (5 cm depth), atmosphere and soil surface, and dew point temperature; (G and H) photosynthetically active radiation (PAR). The yellowish shaded areas highlight daytime (i.e. positive PAR).

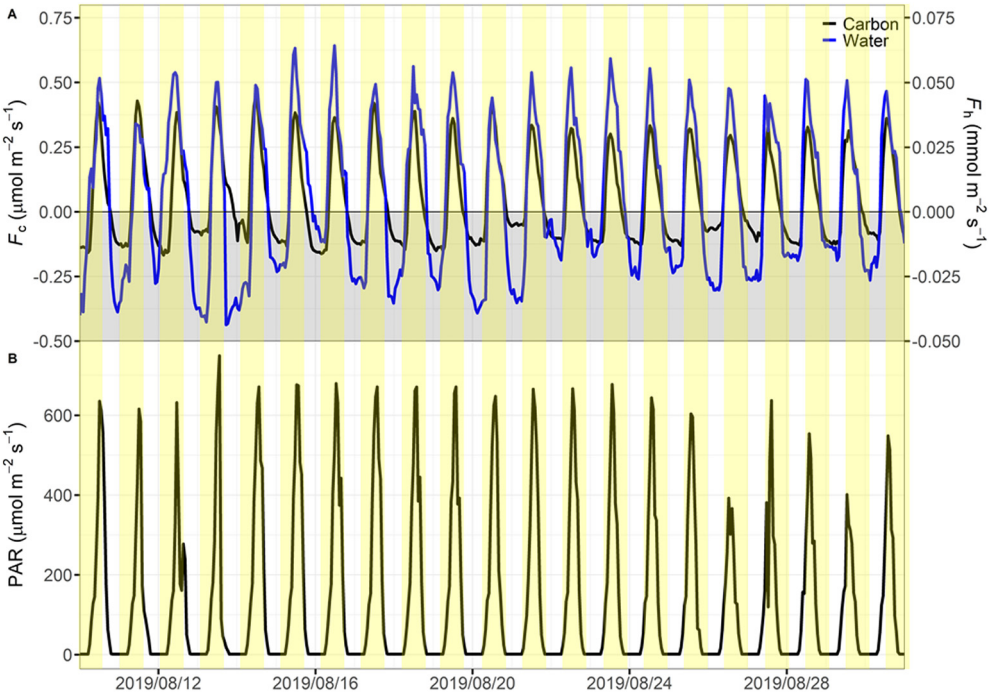

Fig. 4. (A) Covariation between the soil-atmosphere CO_2 flux (F_c) and the soil-atmosphere water vapor flux (F_h) during a selected period in summer; (B) variation in photosynthetically active radiation (PAR) during the same period The dark shaded area highlights negative fluxes. The yellowish areas highlight daytime (i.e. positive PAR). Data were from the *Lepraria isidiata* (LI) microsite.

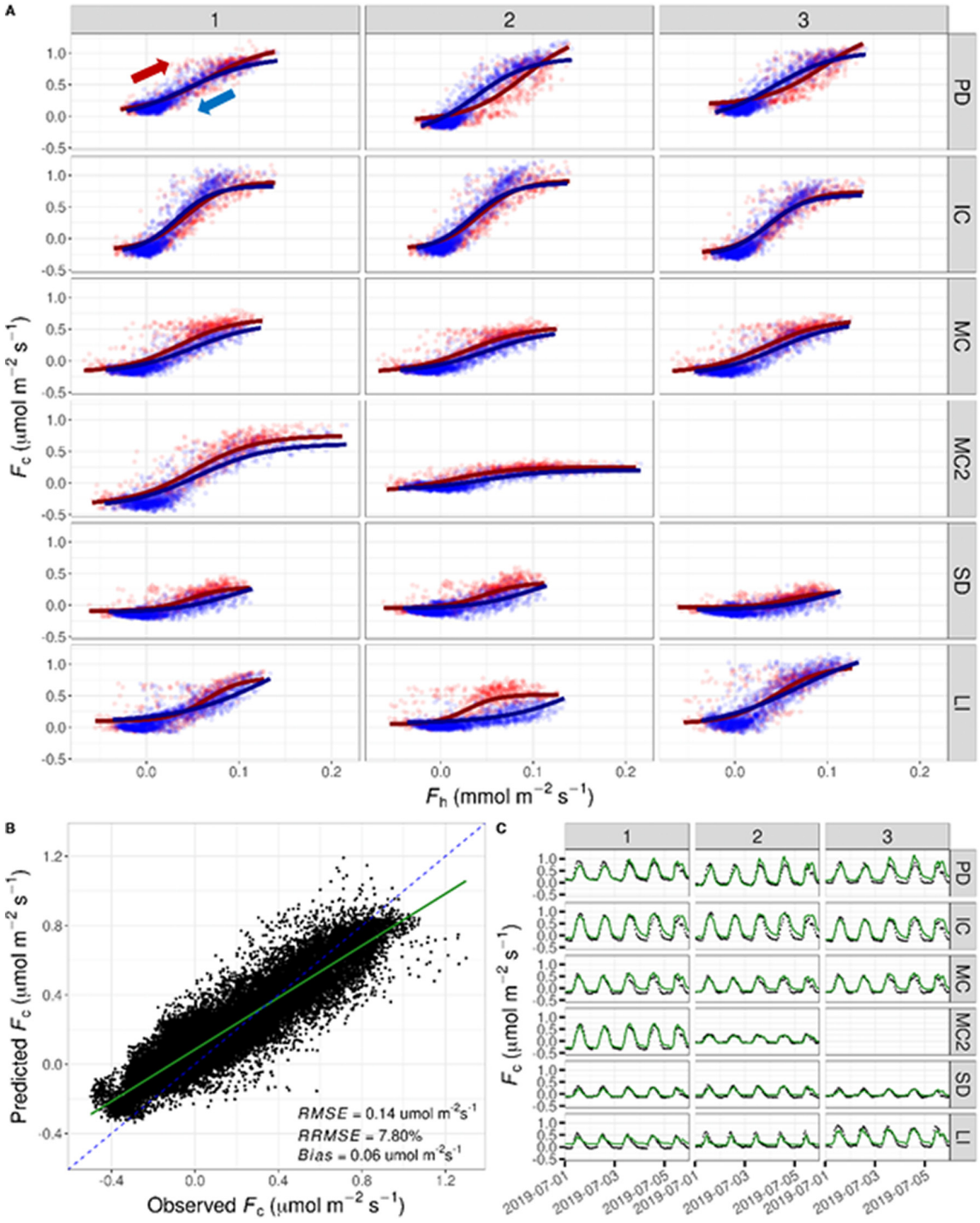

Fig. 5. Non-linear modelling of the hysteretic relationship between the soil-atmosphere CO_2 flux (F_c) and the soil-atmosphere water vapor flux (F_h): (A) calibration of the model on the first summer of data. The blue lines and blue points correspond to the decrease from F_h maximum to minimum and vice-versa for the red line and red points. A summary of the model fixed effects is given in Table S2A; (B) Predicted F_c against observed F_c on the second summer of data for all microsites. The continuous green line is the model. The dashed blue line is the 1:1 line. (C) Example of predicted F_c against time during the second summer of data. The continuous green line is the model prediction. Black points correspond to the observed F_c. Stages of the biocrusts succession are labeled as: physical depositional crust (PD), incipient *Cyanobacteria* (IC), mature *Cyanobacteria* (MC), lichen community dominated by *Squamarina lentigera* and *Diploschistes diacapsis* (SD), lichen community characterized by *Lepraria isidiata* (LI), and *Cyanobacteria* patches within the SD microsite (MC2).

emissions (very close to neutrality) and greatest water vapor emissions. By contrast, the *Lepraria isidiata* microsite exhibited the greatest CO_2 emissions and the least water vapor emissions. The other microsites exhibited intermediate values for these two variables. More details about the temporal patterns of cumulative total fluxes and cumulative negative fluxes for each stage of the succession can be found in Fig. S4. A particular covariation between cumulative negative F_c and F_h was found in the SD microsite with enhanced CO_2 influxes coinciding with water vapor influxes in summer (Fig. S4A).

There was a significant positive linear relationship ($p < 0.001$, adjusted $R^2 = 0.85$) between cumulative CO_2 influxes and total soil specific surface area (SSA_s) among early successional stages (Fig. 7). In other words, the

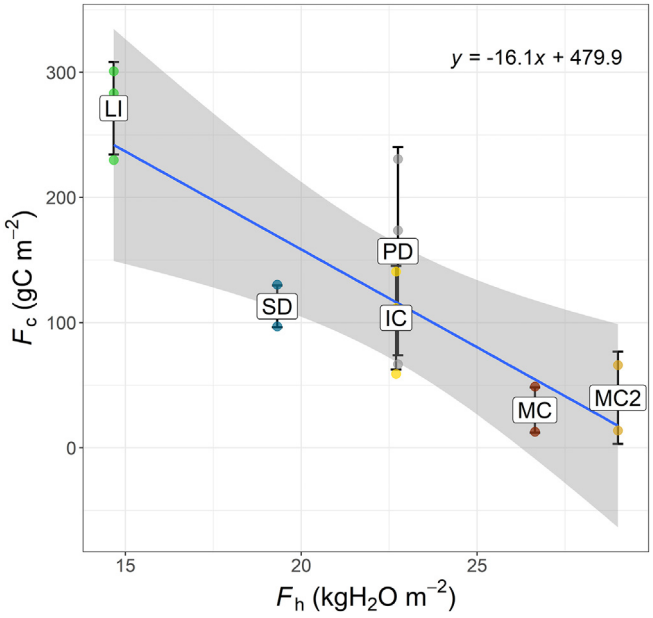

Fig. 6. Fit of the linear model of the cumulative soil-atmosphere CO_2 flux (F_c) as a function of the cumulative soil-atmosphere water vapor flux (F_h), over the whole study period. Stages of the biocrusts succession are labeled as: physical depositional crust (PD), incipient *Cyanobacteria* (IC), mature *Cyanobacteria* (MC), lichen community dominated by *Squamarina lentigera* and *Diploschistes diacapsis* (SD), lichen community characterized by *Lepraria isidiata* (LI), and *Cyanobacteria* patches within the SD microsite (MC2). Grey, yellow, red, orange, blue and green points correspond to the PD, IC, MC, MC2, SD and LI sites, respectively. Error bars represent the intra-microsite standard deviation for F_c. The shaded band represent the 95% confidence interval.

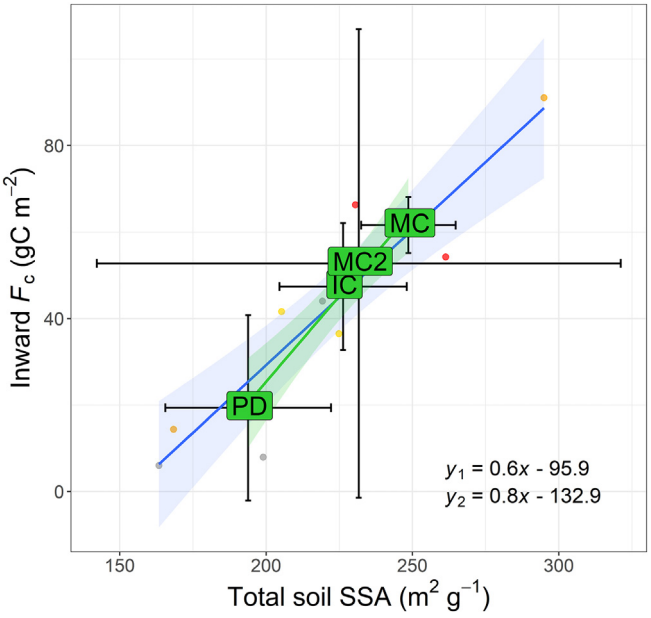

Fig. 7. Fits of linear models of the absolute cumulative inward soil-atmosphere CO_2 flux (F_c) as a function of the total soil specific surface area. The blue and green lines are the model fits from the whole dataset and from averages by crust, respectively (corresponding to the y_1 and y_2 equations, respectively). Stages of the biocrusts succession are labeled as: physical depositional crust (PD), incipient *Cyanobacteria* (IC), mature *Cyanobacteria* (MC), and *Cyanobacteria* patches within a lichen site (MC2). Grey, yellow, red and orange points correspond to data from the PD, IC, MC and MC2 microsites, respectively. Error bars correspond to the intra-microsite standard deviation. Shaded bands represent the 95% confidence intervals. The high spatial variation in the MC2 microsite is attributable to soil heterogeneity and less replicates ($n = 2$ for MC2 and $n = 3$ for other microsites).

magnitude of the CO_2 influxes increased with SSA_s. This proportional increase was observed gradually during the early stages of the succession (from the physical depositional crust to incipient *Cyanobacteria* to mature *Cyanobacteria*). The SSA_s was strongly correlated with the soil clay fraction (Pearson's $r = 0.92$).

There was a significant positive linear relationship ($p < 0.001$, adjusted $R^2 = 0.53$) between the clay fraction and the reactive surface area of calcite (RSA) (Fig. 8A). The RSA was strongly correlated to the calcium carbonate equivalent content (CCE) (Pearson's $r = 0.91$). There was a sigmoidal relationship (relative root mean square error (*RMSE*) = 1.4%) between the CCE and the soil organic carbon content (SOC) within early stages of the succession (Fig. 8B, supporting information Table S2B), that did not follow the order of the succession.

4. Discussion

In this research, we report for the first time using the gradient method (1) negative water vapor fluxes at night during hot and dry periods, attributable to water vapor adsorption (WVA) by soil; (2) a tight coupling between soil-atmosphere CO_2 and water vapor fluxes (F_c and F_h, respectively), and (3) significant relationships between F_c, soil properties and biocrust ecological succession.

4.1. The gradient method as a novel approach to estimate water vapor adsorption by soil

Using the gradient method, negative F_h were consistently and predominantly detected at night during hot and dry periods (i.e. summer) (Fig. 2C). In congruence with this result, in-situ studies have reported that WVA occurs predominantly in those conditions (Agam and Berliner, 2006; Kool et al., 2021; Kosmas et al., 1998). In addition, negative F_h always occurred at $RH_a >$ ca. 40% (Fig. S3). In agreement with this result, according to theoretical equations, a water film starts to form on a solid surface at $RH >$ 30–40% (Kharitonova et al., 2010). Therefore, our observations match those of both in-situ and theoretical studies, thus confirming that our measured negative F_h are attributable to WVA. However, the use of *RH* alone can be misleading to disentangle the temporal patterns involved in WVA in-situ as it is based on the saturation water vapor pressure of air which varies with temperature. By contrast, our results, using the water vapor molar fraction (χ_h) in soil and atmosphere to estimate F_h, provided a more accurate understanding of the underlying processes involved in WVA, as χ_h is independent of temperature, which can vary substantially between soil and atmosphere (Figs. 2F, 3E and F). As a result, soil χ_h and *RH* exhibited opposite diel patterns, and thus the observation of *RH* alone could lead to misleading conclusions. It has been previously stated that WVA occurs when RH_s is lower than RH_a (Agam and Berliner, 2006) and can be attributed to soil drying during daytime and an increase in RH_a at nighttime (Kosmas et al., 1998). However, although WVA occurred during a phase of decreasing χ_h during afternoon and overnight (Fig. 3C), it could not be due to soil drying since both temperature and PAR were decreasing during those moments. On the light of our results, the observed diel decrease in soil χ_h can be attributed to lower temperature reducing the capacity of air to store water vapor.

Furthermore, during an unusually dry period in winter, the soil water content (ϑ_w) decreased to values similar to those observed during summer (Fig. 2E) but soil χ_h decreased to values even lower in average than during summer due to the same physical process, i.e. low temperature decreasing the saturation water vapor pressure of air (Fig. 2B and F). In spite of that, WVA were scarce and of small magnitude in winter because atmosphere χ_h was also lower in average than in summer and did not increase enough at night to exceed soil χ_h (Fig. 3D). Therefore, the decrease in soil χ_h alone does not seem sufficient to trigger WVA. Two additional conditions seem to be critical for the process to occur: (1) a substantial average atmosphere χ_h and (2) a sharp and substantial increase in atmosphere χ_h at night. The first condition can be fulfilled in summer due to greater temperature triggering

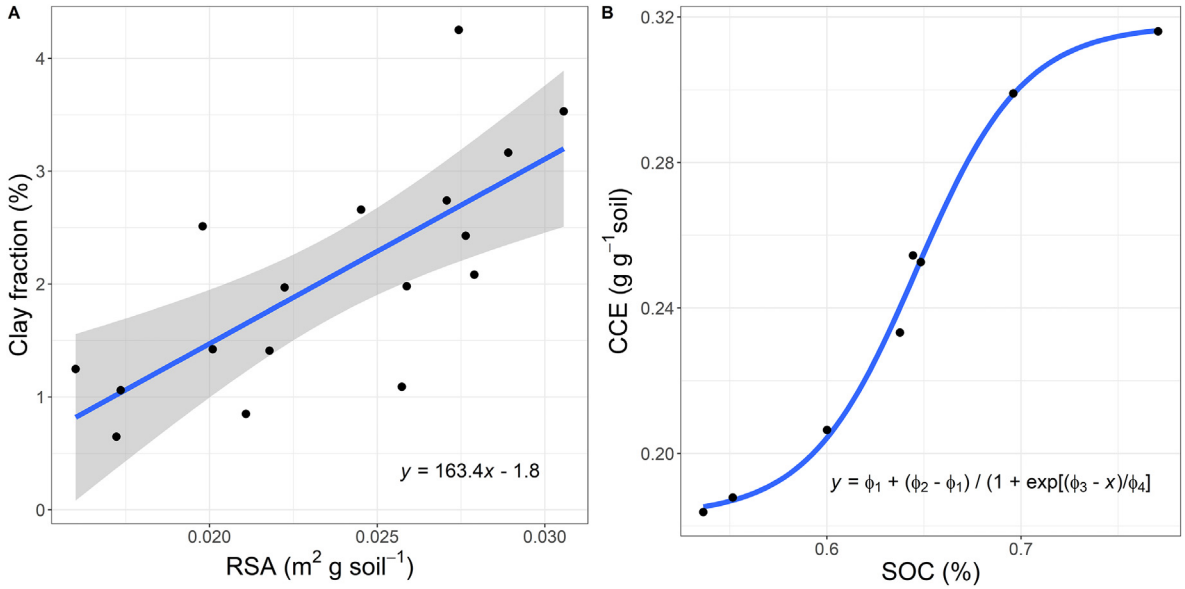

Fig. 8. Fits of (A) linear model of the soil clay fraction as a function of the reactive surface area of calcite (RSA). The shaded band represent the 95% confidence interval, (B) non-linear model of the calcium carbonate equivalent content (CCE) as a function of soil organic carbon content (SOC). Values of the parameters of the model are given in Table S2B.

more oceanic evaporation and as previously explained, the increased capacity of warmer air to store water vapor. Most studies reporting WVA fluxes were conducted in coastal drylands (e.g. Kohfahl et al., 2021; Kool et al., 2021; Kosmas et al., 2001), where atmosphere is usually wetter. Our study site was also close to the sea (ca. 20 km, see Fig. S1). Therefore, further research is needed to clarify if WVA can also occur in non-coastal drylands. The second condition is most likely met due to stable stratification of the atmosphere boundary layer at night accumulating water molecules in the vapor form close to the ground. Previous studies have stated that such nocturnal conditions might be fulfilled due to incoming sea breeze at night (Kosmas et al., 2001; Uclés et al., 2015). However, since sea breeze is a daytime process, it seems rather unlikely at our site. By contrast, here, the movement of wetter air from the surrounding mountains could also have played a role in explaining the sharp increase in atmosphere χ_h at night. We also suggest that the early morning peak in atmosphere χ_h, coinciding with the rise in PAR (Fig. 3C and G), is due to rapid soil surface evaporation at sunrise. This movement of water vapor from soil surface to the overlying low part of the atmosphere only occurs briefly probably because sun radiation rapidly heats the soil surface (Fig. 3E), thus triggering atmospheric turbulences that moves water vapor to higher atmosphere layers.

To our knowledge, it is the first time that the gradient method has been used to estimate WVA. Other approaches traditionally used either complex numerical modelling with numerous parameters that require substantial effort to collect, or expensive lysimeters that can disturb the natural soil profile and pedoclimatic conditions (Agam and Berliner, 2006; Kohfahl et al., 2021; Kosmas et al., 2001; Saaltink et al., 2020; Uclés et al., 2015; Verhoef et al., 2006). By contrast, the gradient method traditionally used to determine soil-atmosphere greenhouse gas fluxes (Maier and Schack-Kirchner, 2014; Sánchez-Cañete et al., 2017) is easy to deploy, generates only limited perturbation of the soil profile, and can provide long-term continuous low-cost measurements and further understanding of belowground mechanisms involved in WVA. It is therefore suitable to obtain estimates of WVA, based on the assumption that all the water vapor that diffuses from atmosphere to soil is adsorbed onto soil particles. The values estimated in this study ranging from 0.21 ± 0.01% to 0.91 ± 0.05% of annual precipitation should be considered as a proxy rather than absolute estimates of WVA because they are highly dependent on the selected model of water vapor diffusion. For example, using a different diffusion model (Xu et al., 1992), our WVA estimates ranged this time from 0.82 ± 0.04% to 2.82 ± 0.14% of the annual precipitation. This difference in the estimated WVA is thus the result of potential errors in the quantification of F_h attributable to the choice of the diffusion model. That is because in the gradient method, the estimated flux is highly dependent on the chosen coefficient of diffusion. Whereas the diffusion coefficient used to estimate F_c was calibrated empirically with a portable soil chamber according to Sánchez-Cañete et al. (2017), no standardized procedure exists yet to calibrate this coefficient in-situ for F_h as, so far, most studies were limited to laboratory experiments (e.g. Jabro, 2008; Rao and Rekapalli, 2020; Reyzabal and Bazán, 1992). In order to obtain reliable absolute estimates of WVA, we suggest to calibrate the diffusion model with another validated method, e.g. using lysimeter measurements. However, since the main objectives of this research were to identify moments of WVA as well as their drivers and potential interactions with F_c, the use of a general model to estimate the coefficient of diffusion of water vapor was reasonable; it was still useful to compare the magnitude of WVA between microsites, analyze temporal patterns and explore correlations with other variables. Although our estimated contribution of WVA to annual precipitation is apparently small, WVA was barely the only source of water in summer when microclimatic conditions necessary for other non-rainfall water inputs, i.e. fog or dew formation, were uncommon. Hence, this water input is likely important for maintaining ecosystem processes during those periods. Our estimated values of evaporation (positive F_h) accounted for up to 30.9% of annual precipitation, indicating that the water balanced was not closed regardless of the diffusion model that was used. The remaining water could have (1) been lost by runoff; (2) infiltrated deeper horizons and (3) been consumed by biocrusts and geochemical reactions.

4.2. Coupling between water vapor and CO_2 fluxes

4.2.1. Coupling between fluxes on a diel scale

During summer, F_c and F_h used to be both negative at night (Fig. 4) and our cross-correlation analysis revealed that the variation in F_h tended to slightly lead the variation in F_c (by 1 h). This is in agreement with our hypothesis that WVA could be the underlying process controlling nocturnal CO_2 uptake in dry soils at this site, but due to the small lag corresponding to the maximum time resolution of the data, this result should be taken with caution and requires further confirmation with higher sampling frequency.

A diel hysteresis between F_c and T_s as well as between F_c and F_h was found (supplementary material Fig. S2A and B, and Fig. 5A). The former

has been extensively described in plants and generally attributed to a lag in the delivery of recent photosynthates to the soil (Dusza et al., 2020; Zhang et al., 2018), stimulating microbial activity, a process known as "priming effect" (Guenet et al., 2018); priming effect mediated by biocrusts has been less studied but does occur (Beymer and Klopatek, 1991). However, this relationship between F_c and T_s was difficult to model in our study. By contrast, the hysteresis between F_c and F_h could be modelled with two sigmoidal functions, one for the diel decrease from maximum to minimum F_h and vice-versa for the diel increase (Fig. 5A, supporting information Table S2A), and the models performed well at predicting F_c from a new dataset (Fig. 5B and C). A lag due to a priming effect induced by biocrusts is possible to a certain extent as a fraction of their photosynthates is assimilated by the underlying microbial community, benefiting heterotrophic microbes which are often carbon-limited in drylands (Belnap et al., 2003). However, the duration of this lag is expected to be limited due to the absence of large phloem structures to transport those photosynthates such as in plants (Mencuccini and Hölttä, 2010). In addition, biocrusts gross photosynthesis is almost inexistent during the dry season at our site (Miralles et al., 2018) and the hysteresis was observed even in the absence of biocrusts, in the physical depositional crust. We therefore suggest that an abiotic mechanism depending on F_h could be involved in the hysteresis between F_c and F_h. Adsorption-desorption of water vapor on solid particles is a good candidate process as it exhibits a well-known hysteresis which is considered to be crucial for accurate modelling of water vapor flow in drylands soils (Arthur et al., 2020). It has been reported from ex-situ experiments on soils that the adsorption time was always greater than the desorption time, with ratios of adsorption time to desorption time ranging from 1.3 to 2.9 (Akin and Likos, 2020). Here we found that the diel "decrease" path of the observed hysteresis was always longer than the diel "increase" path, with ratios of the decrease time to increase time ranging from 1.6 to 3, thus matching closely the previous values; we therefore further assume that the observed paths of "decrease" and "increase" were likely due to underlying adsorption and desorption processes, respectively.

Noteworthy, the hysteresis reported in Arthur et al. (2020) characterizes the relation between ϑ_w and relative humidity, whereas our assumption that water vapor adsorption and desorption processes are involved is based on the relation between F_c and F_h. Our ϑ_w measurements did not provide enough diel resolution to confirm the former relationship. However, we assume that a greater water content during the desorption phase that during the adsorption phase (Arthur et al., 2020) should enhance F_c in this water-limited ecosystem, and therefore that it could generate the observed hysteresis exhibiting greater F_c during the hypothetical desorption phase at most microsites (Fig. 5A). In addition, during the hypothetical adsorption phase, fluxes became negative only at the end of the curve. We suggest that this might be due to (1) a threshold effect (Kharitonova et al., 2010) and/or (2) different thermal conditions between laboratory and in-situ studies. Although similitudes can be found comparing observations of laboratory and in-situ measurements, they are only comparable to a certain extent as laboratory results are usually based on isotherms whereas temperature is not constant in the field but seems to be the motor of WVA (Fig. 3E). Therefore, we suggest that incubations of dry soils placed on lysimeters at constant temperature and varying *RH*, or in-situ temperature and *RH* manipulation could help to validate our assumption.

The abiotic process of WVA could have affected F_c, contributing to a nocturnal CO_2 uptake in different ways, enhancing other abiotic processes and/or biotic processes. Abiotic processes likely to be enhanced by WVA include (1) dissolution of CO_2 in water; (2) mineral reactions such as dissolution of the surface of $CaCO_3$ particles, consuming CO_2 through the following reversible geochemical reaction:

$$CaCO_{3\,(s)} + H_2O_{(l)} + CO_{2\,(g)} \leftrightarrow Ca^{2+} + 2HCO_3^- \quad (11)$$

It has been shown that WVA on the surface of calcite is energetically favorable and that adsorbed water can affect particle reactivity by enhancing surface ion mobility, by providing a medium for reactions or by serving as a reactant in surface-catalyzed hydrolysis reactions (Rahaman et al., 2008). Moreover, much evidence has already supported such a geochemical origin for the nighttime CO_2 uptake at this site (Lopez Canfin et al., n.d.). Alternatively, due the co-occurrence of gypsum with calcite and the greater solubility of the former (exceeding calcite by two orders of magnitude), its potential interaction through a common ion effect deserves to be investigated as calcite precipitation from Ca^{2+} released by gypsum could act as a carbon sink (Yu et al., 2019); that is because although calcite precipitation releases 1 mol of CO_2, it still consumes 2 mol of CO_2 as bicarbonate (Eq. (11)); (3) co-adsorption of CO_2. In the presence of equilibrium pressures of water vapor above 1% RH, co-adsorbed water enhances CO_2 adsorption and influences the chemical nature of the predominant adsorbed product from bicarbonate, which is no longer formed, to carbonate (Rubasinghege and Grassian, 2013). Note that if co-adsorption occurs on calcite, this process could potentially push Eq. (11) to the right. In a desert soil with low inorganic carbon content (ca. 4%), it has been reported through an isotope labeling experiment that most of the labeled atmospheric CO_2 was retained in the soil solid phase (Liu et al., 2015). The authors found that the CO_2 may be conserved in certain minerals but did not discuss adsorption as an explanatory process, though WVA can lead to the reorganization of mineral surfaces and the formation of "ice-like" structures (i.e. similar to solid water) (Rubasinghege and Grassian, 2013). It has been estimated that CO_2 adsorption on mineral and soil surfaces can account for 1–3% of the average annual North American terrestrial carbon sink and that the greatest increases are predicted in regions with lower soil CO_2 concentrations (like at our study site), because soils and rock in these regions have a larger proportion of unused adsorption sites (Davidson et al., 2013).

Biotic processes likely to be enhanced by WVA include (1) WVA could stimulate microbial activity of chemotrophs on the surface of soil particles. Other authors have found that WVA increased soil CO_2 production revealing that dryland microorganisms were able to use this water input to sustain their metabolic activity (McHugh et al., 2015). Since there is growing evidence that chemotrophs that are able to perform CO_2 fixation in the dark are present among biocrust communities in drylands (Bay et al., 2021; Liu et al., 2021), WVA could enhance the activity of these organisms that consume CO_2 at night. Moreover, as negative fluxes of water vapor and CO_2 used to start exactly when PAR reached zero values (Figs. 3 and 4), the hypothesis of dark fixation by chemotrophs deserves further investigation. Note that we measured maximal CO_2 uptake below *Cyanobacteria* (Fig. S4A). Those microorganisms could also promote the dissolution of calcite as they are able to decrease the local extracellular ion activity product of $CaCO_3$ by taking up Ca^{2+}, the weathering capacity of *Cyanobacteria* being optimal in the presence of a short daily dark phase (Garcia-Pichel et al., 2010); (2) WVA could favor the biomineralization of $CaCO_3$ from atmospheric CO_2, either by stimulating the activity of biomineralizing microorganisms or indirectly through the formation of dissolved inorganic carbon species involved in the process. Biomineralization has been frequently identified in *Actinobacteria*, and *Proteobacteria* phyla (Cuezva et al., 2012; Hervé et al., 2016; Meier et al., 2017) including in desert soils (Liu et al., 2018) as well as in *Cyanobacteria* (Benzerara et al., 2014). Those phyla were abundant at our study site (Miralles et al., 2020) and thus deserve further attention in future research.

4.2.2. Coupling between cumulative fluxes

A significant negative linear relationship between total cumulative F_c and F_h over the study was identified (Fig. 6), with minimum CO_2 emissions occurring in mature *Cyanobacteria* microsites, where water vapor emissions were maximum. Those microsites were also the driest, as they exhibited minimum average values of soil water content (not shown). They also sustained the greatest magnitude of soil CO_2 uptake (Fig. S4A). Therefore, one the one hand, the low liquid water availability in *Cyanobacteria* microsites was related to greater water vapor losses from soil to atmosphere, thus probably limiting microbial activity and CO_2 production. On the other hand, the greater CO_2 uptake in mature *Cyanobacteria* microsites contributed to mitigate CO_2 emissions there.

We did not find any significant relationship between annual cumulative negative F_c and F_h, most likely because negative F_c occurred over the whole study period, whereas WVA occurred mainly in summer (Fig. 2C and D) and/or because of high intra-microsite variation in F_h that was not captured by our measurements. However, the significant relationship between total cumulative F_c and F_h deserves additional research integrating more years of data and more spatial coverage for F_h in order to cross-validate a model. A predictive model of annual F_c from annual F_h would present the enormous advantage of providing annual estimates of a variable that is relatively costly to measure (i.e. F_c) from a variable that is very affordable to measure (i.e. F_h).

4.3. Effect of soil properties on water vapor adsorption

We found a strong positive linear relationship between cumulative CO_2 influxes and total soil specific surface area (SSA_s) among early successional stages (Fig. 7). The controlled adsorption of gases on surfaces through the Brunauer-Emmett-Teller (BET) technique is widely used to measure the surface area of solid materials, as adsorption increases with surface area. Therefore, many porous materials of high surface area - clays, carbonates and volcanic residues - have been investigated in laboratory conditions for their adsorbent properties to capture CO_2 (Davidson et al., 2013; Ouadjenia et al., 2017). However, to our knowledge, this relationship between soil CO_2 uptake and surface area has never been evidenced in-situ. It could result from (1) direct adsorption of CO_2 onto soil particles; (2) an indirect effect of WVA enhancing CO_2 adsorption or triggering the dissolution of CO_2 in the adsorbed water; (3) enhanced chemotrophs/biomineralizers growth due to more available surface area and/or water.

We found no convincing relationship between cumulative negative F_h and SSA_s to confirm an indirect role of WVA. However, that was likely due to the lack of intra-microsite replicates of relative humidity measurements to capture the spatial variability of F_h, and thus this assumption should not be discarded. The absence of consistent relationship between cumulative CO_2 influxes and SSA_s in late succession stages is most likely due to higher CO_2 production masking CO_2 consumption in those microsites. Other factors such as soil organic carbon (SOC) and salinity could also have affected adsorption (Amer, 2019; Arthur et al., 2020; Ravikovitch et al., 2005), but we did not find evidence of such relationships between adsorption and those parameters (including the content of a common salt, gypsum) at our site.

Furthermore, the strong relationship between SSA_s and clay fraction indicates that this soil CO_2 uptake was related to clay particles. Even if clays were not abundant at this site (ranging from 0.6 to 4.3% in the measured samples), they contained highly adsorbent smectite (Hatch et al., 2012; Michels et al., 2015). Although smectite could have contributed to a certain extent to adsorption, its contribution was probably limited since it was only present in minor amounts (<5% of the clay fraction) (Solé-Benet et al., 1997). However, we found a significant relationship between the clay fraction and the reactive surface area of carbonates (RSA) (Fig. 8A), suggesting that there was a substantial amount of clay-size carbonate at this site. Clay-size carbonates are highly reactive (Loeppert and Suarez, 1996) and thus might have reacted with adsorbed CO_2 and/or water according to Eq. (11).

4.4. Effect of biocrusts ecological succession on water vapor adsorption

The ratio of cumulative negative to positive F_h and the average soil-atmosphere gradient of water vapor molar fraction respectively increased and decreased over biocrust ecological succession, suggesting that those variables might be used as indices of succession status. However, further research is needed to explore the potential biophysical mechanisms controlling those patterns.

In early successional stages, the SSA_s increased following the order of ecological succession (physical depositional crust – incipient *Cyanobacteria* – mature *Cyanobacteria*) and was associated with an increase in the magnitude of soil CO_2 uptake (Fig. 7). In agreement with those results, on sandy soils, biocrusts are known to accumulate windblown silt and clay particles at the surface, and clay particles in particular may be tightly bound to the sticky sheaths of some *Cyanobacteria* (Warren, 2003); therefore, *Cyanobacteria* could indirectly favor WVA by accumulating fine particles. Moreover, at our experimental site, the dominance of *Cyanobacteria* in the driest microsites though those organisms require liquid water to develop is somewhat paradoxical. Since the greatest magnitude of summer WVA was observed in the mature cyanobacterial microsite (Fig. S4A), it is possible that *Cyanobacteria* take advantage of enhanced WVA in the driest microsites and use adsorbed water films to develop. Furthermore, as those organisms have the size of fine-silt particles, it is also possible that they favor WVA by providing additional adsorbent surface, surface that would be free for more adsorption once the water has been consumed by the microorganisms, thus generating a positive feedback loop between WVA and their development. Other authors have found that WVA capacity was increased by up to 157% in moss-dominated soils compared to bare soils (Li et al., 2021), hence this assumption regarding *Cyanobacteria* deserves further research. The enhanced CO_2 uptake by soil coinciding with WVA in the SD lichen community during summer also requires further investigation to clarify the involved processes (Fig. S4A).

The logistic relationship found within early successional stages between the calcium carbonate equivalent content and SOC (Fig. 8B, supporting information Table S2B) is assumed to be due to the cementing effect of carbonates on aggregates (Rowley et al., 2018). Therefore, $CaCO_3$ might be crucial to stabilize organic matter in early successional stages. In late stages, other factors might contribute to organic carbon accumulation such as lichen and plant turnover and secretion of organic compounds. In agreement with those results, a previous study at this experimental site has found a trend of increase in small-size carbonates over succession (Lopez-Canfin et al., 2021). Those particles could potentially affect F_h and F_c due to their highly adsorbent and reactive properties. Additional research is needed to determine if this accumulation of small-size carbonates has an abiotic origin (through mineral dissolution and precipitation processes) or is mediated by biocrusts (e.g. through interception of fine particles or biomineralization).

5. Conclusions

In conclusion, this study identified for the first time WVA periods with the gradient method and provided further understanding on the underlying processes involved in the temporal patterns (diel and seasonal) of WVA. We also found that WVA was the main source of water in summer when microclimatic conditions necessary to other non-rainfall water inputs were uncommon. Our main finding is the existence of a tight coupling between F_c and F_h. So far, F_c has commonly been modelled as a function of T_s, ϑ_w and proxies of photosynthesis. Here, for the first time, F_c was modelled as a function of F_h during summer, providing robust predictions and thus this relation deserves to be tested in other ecosystems. We attribute the detected diel hysteresis between F_c and F_h to a potential water vapor adsorption/desorption process. The occurrence of both CO_2 and water vapor uptake by soil at night suggests that both processes might be connected. We propose different biogeochemical mechanisms through which WVA could contribute or interact with this CO_2 uptake, including the potential co-adsorption of those gases on highly reactive clay-size calcite and the potential enhancement of the activity of specialized microorganisms.

More efforts are now needed to confirm the role of WVA on soil CO_2 uptake and disentangle the suggested involved processes, as well as to confirm its occurrence in other non-coastal drylands. In particular, the assumption according to which the soil CO_2 uptake could not arise from calcite dissolution due to the lack of water in drylands, should be revisited, as it did not consider WVA as a potential link between the water and carbon cycle in those environments. Additional research is needed to monitor soil water vapor and CO_2 uptake as those sinks could grow with climate change in different ways: (1) warmer air has the capacity to hold more water vapor, and a soil drying is predicted in some regions of the globe, thus potentially enhancing WVA; (2) the atmospheric CO_2 increase is expected to enhance CO_2 adsorption by soils, especially in areas of low biological activity (typically,

drylands) and where highly adsorbent phases are present; (3) little is known about the effect of future elevated CO_2 on the rate of CO_2 fixation by microorganisms. In addition, the significance of the water input through WVA in hot and dry conditions leaves the door open for novel or growing research areas, for example to explore the role of WVA on ecosystem processes such as microbial and mineral reactions, on the growth of plants of agricultural interest in drylands, and as a potential source of liquid water in extra-terrestrial environments. Finding ways of optimizing WVA for agriculture in water-limited ecosystems is particularly relevant as they cover about 41% of Earth's terrestrial surface and support more than two billion people (about one third of the world's total population), 90% of whom are in developing countries.

CRediT authorship contribution statement

Clément Lopez-Canfin: Conceptualization, Methodology, Software, Validation, Formal Analysis, Investigation, Data Curation, Writing - Original draft preparation, Visualization. **Roberto Lázaro**: Conceptualization, Methodology, Investigation, Resources, Writing - Review & Editing, Supervision, Project administration, Funding acquisition. **Enrique P. Sánchez-Cañete**: Conceptualization, Methodology, Investigation, Resources, Writing - Review & Editing, Supervision, Project administration, Funding acquisition.

Declaration of competing interest

The authors declare that they have no known competing financial interests or personal relationships that could have appeared to influence the work reported in this paper.

Acknowledgements

This work was funded by the research project CGL2016-78075-P, Biocrust Dinamics (DINCOS), of the Spanish National Program of Scientific and Technical Research, and by the ICAERSA research project (P18-RT-3629) of the Andalusian Regional Government including European Union ERDF funds. We are grateful to Andrew S. Kowalski for the proofreading and insightful suggestions that considerably improved the manuscript, to Consuelo Rubio who performed the particle size analysis; and we are grateful to the Viciana brothers, landowners of the El Cautivo experimental site, without whose kind consent to set up semi-permanent installations on their land, this research would not have been possible. The funding for the open access charge was provided by the University of Granada / CBUA.

Appendix A. Supplementary figures and tables

Supplementary data to this article can be found online at https://doi.org/10.1016/j.scitotenv.2022.153746.

References

Agam, N., Berliner, P.R., 2006. Dew formation and water vapor adsorption in semi-arid environments—a review. J. Arid Environ. 65, 572–590.
Akin, I.D., Likos, W.J., 2017. Implications of surface hydration and capillary condensation for strength and stiffness of compacted clay. J. Eng. Mech. 143, 4017054.
Akin, I.D., Likos, W.J., 2020. Relationship between water vapor sorption kinetics and clay surface properties. J. Geotech. Geoenviron. Eng. 146, 6020015.
Amer, A.M., 2019. Soil moisture adsorption capacity and specific surface area in relation to water vapor pressure in arid and tropical soils. Eurasian J. Soil Sci. 8, 289–297. https://doi.org/10.18393/EJSS.580889.
Arthur, E., Tuller, M., Moldrup, P., de Jonge, L.W., 2020. Clay content and mineralogy, organic carbon and cation exchange capacity affect water vapour sorption hysteresis of soil. Eur. J. Soil Sci. 71, 204–214.
Azimi, G., Papangelakis, V.G., Dutrizac, J.E., 2007. Modelling of calcium sulphate solubility in concentrated multi-component sulphate solutions. Fluid Phase Equilib. 260, 300–315.
Bay, S.K., Waite, D.W., Dong, X., Gillor, O., Chown, S.L., Hugenholtz, P., Greening, C., 2021. Chemosynthetic and photosynthetic bacteria contribute differentially to primary production across a steep desert aridity gradient. ISME J. 1–18.
Belnap, J., Prasse, R., Harper, K.T., 2003. Influence of biological soil crusts on soil environments and vascular plants. Biological Soil Crusts: Structure, Function, and Management. Springer, Berlin, Heidelberg, pp. 281–300 https://doi.org/10.1007/978-3-642-56475-8_21.
Benzerara, K., Skouri-Panet, F., Li, J., Férard, C., Gugger, M., Laurent, T., Couradeau, E., Ragon, M., Cosmidis, J., Menguy, N., 2014. Intracellular ca-carbonate biomineralization is widespread in cyanobacteria. Proc. Natl. Acad. Sci. 111, 10933–10938.
Beymer, R.J., Klopatek, J.M., 1991. Potential contribution of carbon by microphytic crusts in pinyon-juniper woodlands. Arid Land Res. Manag. 5, 187–198. https://doi.org/10.1080/15324989109381279.
Bittelli, M., Campbell, G.S., Tomei, F., 2015. Soil Physics With Python: Transport in the Soil-plant-atmosphere System. OUP Oxford.
Bittelli, M., Ventura, F., Campbell, G.S., Snyder, R.L., Gallegati, F., Pisa, P.R., 2008. Coupling of heat, water vapor, and liquid water fluxes to compute evaporation in bare soils. J. Hydrol. 362, 191–205. 10.1016/J.JHYDROL.2008.08.014.
Buck, A.L., 1981. New equations for computing vapor pressure and enhancement factor. J. Appl. Meteorol. 20, 1527–1532.
Campbell, G.S., Norman, J.M., 1998. An Introduction to Environmental Biophysics. An Introd. to Environ. Biophys. https://doi.org/10.1007/978-1-4612-1626-1.
Cantón, Y., Solé-Benet, A., Lázaro, R., 2003. Soil–geomorphology relations in gypsiferous materials of the Tabernas Desert (Almeria, SE Spain). Geoderma 115, 193–222. https://doi.org/10.1016/S0016-7061(03)00012-0.
Collins, M., Knutti, R., Arblaster, J., Dufresne, J.-L., Fichefet, T., Friedlingstein, P., Gao, X., Gutowski, W.J., Johns, T., Krinner, G., 2013. Long-term climate change: projections, commitments and irreversibility. Climate Change 2013-The Physical Science Basis: Contribution of Working Group I to the Fifth Assessment Report of the Intergovernmental Panel on Climate Change. Cambridge University Press, pp. 1029–1136.
Cuezva, S., Fernandez-Cortes, A., Porca, E., Pašić, L., Jurado, V., Hernandez-Marine, M., Serrano-Ortiz, P., Hermosin, B., Cañaveras, J.C., Sanchez-Moral, S., 2012. The biogeochemical role of Actinobacteria in Altamira cave, Spain. FEMS Microbiol. Ecol. 81, 281–290.
Davidson, G.R., Phillips-Housley, A., Stevens, M.T., 2013. Soil-zone adsorption of atmospheric CO2 as a terrestrial carbon sink. Geochim. Cosmochim. Acta 106, 44–50.
Dusza, Y., Sanchez-Cañete, E.P., Le Galliard, J.-F., Ferriere, R., Chollet, S., Massol, F., Hansart, A., Juarez, S., Dontsova, K., Van Haren, J., 2020. Biotic soil-plant interaction processes explain most of hysteretic soil CO 2 efflux response to temperature in cross-factorial mesocosm experiment. Sci. Rep. 10, 1–11.
Fa, K.-Y., Zhang, Y.-Q., Wu, B., Qin, S.-G., Liu, Z., She, W.-W., 2016. Patterns and possible mechanisms of soil CO2 uptake in sandy soil. Sci. Total Environ. 544, 587–594. https://doi.org/10.1016/j.scitotenv.2015.11.163.
FAO, 1998. World Reference Base for Soil Resources. Food & Agriculture Org.
Garcia-Pichel, F., Ramírez-Reinat, E., Gao, Q., 2010. Microbial excavation of solid carbonates powered by P-type ATPase-mediated transcellular Ca2+ transport. Proc. Natl. Acad. Sci. 107, 21749–21754. https://doi.org/10.1073/pnas.1011884108.
Guenet, B., Camino-Serrano, M., Ciais, P., Tifafi, M., Maignan, F., Soong, J.L., Janssens, I.A., 2018. Impact of priming on global soil carbon stocks. Glob. Chang. Biol. 24, 1873–1883. https://doi.org/10.1111/gcb.14069.
Hamerlynck, E.P., Scott, R.L., Sánchez-Cañete, E.P., Barron-Gafford, G.A., 2013. Nocturnal soil CO2 uptake and its relationship to subsurface soil and ecosystem carbon fluxes in a Chihuahuan Desert shrubland. J. Geophys. Res. Biogeosci. 118, 1593–1603. https://doi.org/10.1002/2013JG002495.
Hatch, C.D., Wiese, J.S., Crane, C.C., Harris, K.J., Kloss, H.G., Baltrusaitis, J., 2012. Water adsorption on clay minerals as a function of relative humidity: application of BET and Freundlich adsorption models. Langmuir 28, 1790–1803.
Hervé, V., Junier, T., Bindschedler, S., Verrecchia, E., Junier, P., 2016. Diversity and ecology of oxalotrophic bacteria. World J. Microbiol. Biotechnol. 32, 28.
Jabro, J.D., 2008. Water vapor diffusion through soil as affected by temperature and aggregate size. Transp. Porous Media 773 (77), 417–428. 10.1007/S11242-008-9267-Z.
Jones, H.G., 1992. Plants and Microclimate: A Quantitative Approach to Environmental Plant Physiology. Cambridge university press.
Kargas, G., Londra, P., Sgoubopoulou, A., 2020. Comparison of soil EC values from methods based on 1:1 and 1:5 soil to water ratios and ECe from saturated paste extract based method. Water 12 (2020), 1010. https://doi.org/10.3390/W12041010 12, 1010.
Kharitonova, G.V., Vityazev, V.G., Lapekina, S.I., 2010. A mathematical model for the adsorption of water vapor by soils. Eurasian Soil Sci. 43, 177–186.
Kohfahl, C., Saaltink, M.W., Ruiz Bermudo, F., 2021. Vapor flow control in dune sediments under dry bare soil conditions. Sci. Total Environ. 786, 147404. https://doi.org/10.1016/J.SCITOTENV.2021.147404.
Kool, D., Agra, E., Drabkin, A., Duncan, A., Fendinat, P.P., Leduc, S., Lupovitch, G., Nambwandja, A.N., Ndilenga, N.S., Thi, T.N., 2021. The overlooked non-rainfall water input sibling of fog and dew: daily water vapor adsorption on a! Nara hummock in the namib Sand Sea. J. Hydrol. 598, 126420.
Kosmas, C., Danalatos, N.G., Poesen, J., Van Wesemael, B., 1998. The effect of water vapour adsorption on soil moisture content under Mediterranean climatic conditions. Agric. Water Manag. 36, 157–168.
Kosmas, C., Marathianou, M., Gerontidis, S., Detsis, V., Tsara, M., Poesen, J., 2001. Parameters affecting water vapor adsorption by the soil under semi-arid climatic conditions. Agric. Water Manag. 48, 61–78.
Lange, O.L., Kidron, G.J., Budel, B., Meyer, A., Kilian, E., Abeliovich, A., 1992. Taxonomic composition and photosynthetic characteristics of thebiological soil crusts' covering sand dunes in the western Negev Desert. Funct. Ecol. 519–527.
Lange, O.L., Meyer, A., Zellner, H., Heber, U., 1994. Photosynthesis and water relations of lichen soil crusts: field measurements in the coastal fog zone of the Namib Desert. Funct. Ecol. 8, 253. https://doi.org/10.2307/2389909.
Lázaro, R., Alexander, R.W., Puigdefabregas, J., 2000. Cover Distribution Patterns of Lichens, Annuals and Shrubs in the Tabernas Desert, Almería, Spain.

Lázaro, R., Rodrigo, F.S., Gutiérrez, L., Domingo, F., Puigdefábregas, J., 2001. Analysis of a 30-year rainfall record (1967–1997) in semi–arid SE Spain for implications on vegetation. J. Arid Environ. 48, 373–395. https://doi.org/10.1006/jare.2000.0755.

Lázaro, R., Rodríguez-Tamayo, M.L., Ordiales, R., Puigdefábregas, J.R., 2004. El clima. Subdesiertos Almer. Nat. Cine, pp. 62–79.

Lázaro, R., Cantón, Y., Solé-Benet, A., Bevan, J., Alexander, R., Sancho, L.G., Puigdefábregas, J., 2008. The influence of competition between lichen colonization and erosion on the evolution of soil surfaces in the Tabernas badlands (SE Spain) and its landscape effects. Geomorphology 102, 252–266. https://doi.org/10.1016/j.geomorph.2008.05.005.

Lebron, I., Herrero, J., Robinson, D.A., 2009. Determination of gypsum content in dryland soils exploiting the gypsum–bassanite phase change. Soil Sci. Soc. Am. J. 73, 403–411.

Li, S., Xiao, B., Sun, F., Kidron, G.J., 2021. Moss-dominated biocrusts enhance water vapor sorption capacity of surface soil and increase non-rainfall water deposition in drylands. Geoderma 388, 114930.

Liu, J., Fa, K., Zhang, Y., Wu, B., Qin, S., Jia, X., 2015. Abiotic CO2 uptake from the atmosphere by semiarid desert soil and its partitioning into soil phases. Geophys. Res. Lett. 42, 5779–5785.

Liu, Z., Zhang, Y., Fa, K., Zhao, H., Qin, S., Yan, R., Wu, B., 2018. Desert soil bacteria deposit atmospheric carbon dioxide in carbonate precipitates. Catena 170, 64–72.

Liu, F., Mao, X.S., Zhang, J.X., Wu, Q., Li, Y., Xu, C., 2020. Isothermal diffusion of water vapor in unsaturated soils based on Fick's second law. J. Cent. South Univ. 277 (27), 2017–2031. 10.1007/S11771-020-4427-6.

Liu, Z., Sun, Y., Zhang, Y., Feng, W., Lai, Z., Qin, S., 2021. Soil microbes transform inorganic carbon into organic carbon by dark fixation pathways in desert soil. J. Geophys. Res. Biogeosci. 126 (5), e2020JG006047.

Loeppert, R.H., Suarez, D.L., 1996. Carbonate and gypsum. Methods Soil Anal. Part 3 Chem. Methods. 5, pp. 437–474. https://doi.org/10.2136/sssabookser5.3.c15.

Lopez Canfinet al., in review, C. Lopez Canfin R. Lázaro , E.P. Sánchez-Cañete , in review. Disparate responses of soil-atmosphere CO2 exchange to biophysical and geochemical factors over a biocrust ecological succession in the Tabernas Desert. Geoderma.

Lopez-Canfin, C., Sánchez-Cañete, E.P., Lazaro, R., 2021. Development of a new low-cost device to measure calcium carbonate content, reactive surface area in solid samples and dissolved inorganic carbon content in water samples. Methods Ecol. Evol. https://doi.org/10.1111/2041-210X.13579.

Ma, J., Wang, Z.-Y., Stevenson, B.A., Zheng, X.-J., Li, Y., 2013. An inorganic CO2 diffusion and dissolution process explains negative CO2 fluxes in saline/alkaline soils. Sci. Rep. 3, 2025. https://doi.org/10.1038/srep02025.

Maier, M., Schack-Kirchner, H., 2014. Using the gradient method to determine soil gas flux: a review. Agric. For. Meteorol. 192, 78–95.

McHugh, T.A., Morrissey, E.M., Reed, S.C., Hungate, B.A., Schwartz, E., 2015. Water from air: an overlooked source of moisture in arid and semiarid regions. Sci. Rep. 5, 1–6.

Meier, A., Kastner, A., Harries, D., Wierzbicka-Wieczorek, M., Majzlan, J., Büchel, G., Kothe, E., 2017. Calcium carbonates: induced biomineralization with controlled macromorphology. Biogeosciences 14, 4867–4878.

Mencuccini, M., Hölttä, T., 2010. The significance of phloem transport for the speed with which canopy photosynthesis and belowground respiration are linked. New Phytol. 185, 189–203.

Michels, L., Fossum, J.O., Rozynek, Z., Hemmen, H., Rustenberg, K., Sobas, P.A., Kalantzopoulos, G.N., Knudsen, K.D., Janek, M., Plivelic, T.S., 2015. Intercalation and retention of carbon dioxide in a smectite clay promoted by interlayer cations. Sci. Rep. 5, 1–9.

Mingorance, M.D., Barahona, E., Fernández-Gálvez, J., 2007. Guidelines for improving organic carbon recovery by the wet oxidation method. Chemosphere 68, 409–413. https://doi.org/10.1016/j.chemosphere.2007.01.021.

Miralles, I., Ladrón de Guevara, M., Chamizo, S., Rodríguez-Caballero, E., Ortega, R., van Wesemael, B., Cantón, Y., 2018. Soil CO2 exchange controlled by the interaction of biocrust successional stage and environmental variables in two semiarid ecosystems. Soil Biol. Biochem. 124, 11–23. https://doi.org/10.1016/J.SOILBIO.2018.05.020.

Miralles, I., Lázaro, R., Sánchez-Marañón, M., Soriano, M., Ortega, R., 2020. Biocrust cover and successional stages influence soil bacterial composition and diversity in semiarid ecosystems. Sci. Total Environ. 709, 134654. https://doi.org/10.1016/J.SCITOTENV.2019.134654.

Ouadjenia, F., Marouf, R., Schott, J., 2017. Mechanism sorption of carbon dioxide onto dam silt. Cogent Chem. 3, 1300974.

Pinheiro, J.C., Bates, D.M., 2000. Mixed-Effects Models in S and S-Plus. Springer-Verlag New York, New York, NY.

Rahaman, A., Grassian, V.H., Margulis, C.J., 2008. Dynamics of water adsorption onto a calcite surface as a function of relative humidity. J. Phys. Chem. C 112, 2109–2115.

Rao, S.M., Rekapalli, M., 2020. Identifying the dominant mode of moisture transport during drying of unsaturated soils. Sci. Reports 101 (10), 1–9. 10.1038/s41598-020-61302-w.

Ravikovitch, P.I., Bogan, B.W., Neimark, A.V., 2005. Nitrogen and carbon dioxide adsorption by soils. Environ. Sci. Technol. 39, 4990–4995.

Reyzabal, M.L., Bazán, J.C., 1992. A method for measurement of water vapor diffusion in dry soils. Geoderma 53, 105–110. 10.1016/0016-7061(92)90024-2.

Rowley, M.C., Grand, S., Verrecchia, É.P., 2018. Calcium-mediated stabilisation of soil organic carbon. Biogeochemistry 137, 27–49.

Rubasinghege, G., Grassian, V.H., 2013. Role (s) of adsorbed water in the surface chemistry of environmental interfaces. Chem. Commun. 49, 3071–3094.

Saaltink, M.W., Kohfahl, C., Molano Leno, L., 2020. Analysis of water vapor adsorption in soils by means of a lysimeter and numerical modeling. Vadose Zone J. 19, e20012 1-e20012: 18.

Sagi, N., Zaguri, M., Hawlena, D., 2021. Soil CO2 influx in drylands: a conceptual framework and empirical examination. Soil Biol. Biochem. 156, 108209. https://doi.org/10.1016/J.SOILBIO.2021.108209.

Sánchez-Cañete, E.P., Scott, R.L., van Haren, J., Barron-Gafford, G.A., 2017. Improving the accuracy of the gradient method for determining soil carbon dioxide efflux. J. Geophys. Res. Biogeosci. 122, 50–64.

Schlesinger, W.H., Belnap, J., Marion, G., 2009. On carbon sequestration in desert ecosystems. Glob. Chang. Biol. 15, 1488–1490.

Šimůnek, J., Suarez, D.L., 1993. Modeling of carbon dioxide transport and production in soil: 1. Model development. Water Resour. Res. 29, 487–497.

Solé-Benet, A., Calvo, A., Cerda, A., Laïzaro, R., Pini, R., Barbero, J., 1997. Influences of micro-relief patterns and plant cover on runoff related processes in badlands from Tabernas (SE Spain). Catena 31, 23–38.

Stekhoven, D.J., Bühlmann, P., 2012. MissForest—non-parametric missing value imputation for mixed-type data. Bioinformatics 28, 112–118. https://doi.org/10.1093/bioinformatics/btr597.

Tian, D., Su, M., Zou, X., Zhang, L., Tang, L., Geng, Y., Qiu, J., Wang, S., Gao, H., Li, Z., 2021. Influences of phosphate addition on fungal weathering of carbonate in the red soil from karst region. Sci. Total Environ. 755, 142570. https://doi.org/10.1016/J.SCITOTENV.2020.142570.

Uclés, O., Villagarcía, L., Cantón, Y., Lázaro, R., Domingo, F., 2015. Non-rainfall water inputs are controlled by aspect in a semiarid ecosystem. J. Arid Environ. 113, 43–50.

Verhoef, A., Diaz-Espejo, A., Knight, J.R., Villagarcía, L., Fernandez, J.E., 2006. Adsorption of water vapor by bare soil in an olive grove in southern Spain. J. Hydrometeorol. 7, 1011–1027.

Wang, L., Kaseke, K.F., Seely, M.K., 2017. Effects of non-rainfall water inputs on ecosystem functions. Wiley Interdiscip. Rev. Water 4, e1179. https://doi.org/10.1002/WAT2.1179.

Warren, S.D., 2003. Synopsis: influence of biological soil crusts on arid land hydrology and soil stability. Biological Soil Crusts: Structure, Function, and Management. Springer, pp. 349–360.

Xu, X., Nieber, J.L., Gupta, S.C., 1992. Compaction effect on the gas diffusion coefficient in soils. Soil Sci. Soc. Am. J. 56, 1743–1750.

Yu, L., Daniels, L.M., Mulders, J.J.P.A., Saldi, G.D., Harrison, A.L., Liu, L., Oelkers, E.H., 2019. An experimental study of gypsum dissolution coupled to CaCO3 precipitation and its application to carbon storage. Chem. Geol. 525, 447–461. https://doi.org/10.1016/J.CHEMGEO.2019.08.005.

Zhang, Q., Phillips, R.P., Manzoni, S., Scott, R.L., Oishi, A.C., Finzi, A., Daly, E., Vargas, R., Novick, K.A., 2018. Changes in photosynthesis and soil moisture drive the seasonal soil respiration-temperature hysteresis relationship. Agric. For. Meteorol. 259, 184–195.

Zheng, J., Peng, C., Li, H., Li, S., Huang, S., Hu, Y., Zhang, J., Li, D., 2018. The role of non-rainfall water on physiological activation in desert biological soil crusts. J. Hydrol. 556, 790–799. https://doi.org/10.1016/J.JHYDROL.2017.12.003.

Zuur, A.F., Ieno, E.N., 2016. A protocol for conducting and presenting results of regression-type analyses. Methods Ecol. Evol. 7, 636–645. https://doi.org/10.1111/2041-210X.12577.